

wards each other close to the grain boundary. In contrast, the grain interiors revealed an increase in misorientation.

Received: May 13, 2003

- [1] J. D. Livingston, B. Chalmers, *Acta Metall.* **1957**, 5, 322.
- [2] C. Rey, A. Zaoui, *Acta Metall.* **1980**, 28, 687.
- [3] R. E. Hook, J. P. Hirth, *Acta Metall.* **1967**, 15, 535.
- [4] R. E. Hook, J. P. Hirth, *Acta Metall.* **1967**, 15, 1099.
- [5] C. Rey, A. Zaoui, *Acta Metall.* **1982**, 30, 523.
- [6] V. Randle, N. Hansen, D. Juul Jensen, *Philos. Mag. A* **1996**, 73, 265.
- [7] R. K. Davies, V. Randle, *Mater. Sci. Eng. A* **2000**, 283, 251.
- [8] C. Rey, *Rev. Phys. Appl.* **1988**, 23, 491.
- [9] D. Raabe, M. Sachtleber, Z. Zhao, F. Roters, S. Zaefferer, *Acta Mater.* **2001**, 49, 3433.
- [10] M. Sachtleber, Z. Zhao, D. Raabe, *Mater. Sci. Eng. A* **2002**, 336, 81.
- [11] F. Delaire, J. L. Raphanel, C. Rey, *Acta Mater.* **2000**, 48, 1075.
- [12] P. Vacher, S. Dumoulin, F. Morestin, S. Mguil-Touchal, *Proc. Inst. Mech. Eng., Part C: J. Mech. Eng. Sci.* **1999**, 213, 811.

## High-Resolution EBSD Investigation of Deformed and Partially Recrystallized IF Steel

By Ingo Thomas,\* Stefan Zaefferer, Frank Friedel, and Dierk Raabe

**Abstract:** The recrystallization of titanium-alloyed interstitial-free steel (IF steel) has been investigated by high-resolution electron backscattered diffraction (EBSD) measurements and transmission electron microscopy (TEM) observations. The deformed microstructure of the cold rolled material can be subdivided into three different groups. These three types of microstructure are characterized by their orientations and internal local misorientations. The development of these three regions during recrystallization annealing has been observed. Nucleation from  $\gamma$ -fiber orientations but also from other or-

ientations was found. Comparison of EBSD and TEM results indicates some limitations of high-resolution EBSD measurements concerning the observation of subgrain structures.

**Motivation:** IF steels are mainly used as sheets for deep-drawing applications (car bodies, cans etc.) for which a high  $r$  value (ratio of strain in width direction to that in thickness direction) is required, in order to reduce thinning. It is well known that a high  $r$  value is related to a high fraction of crystals with a  $\langle 111 \rangle / \text{ND}$  crystal orientation fiber (called  $\gamma$ -fibre).<sup>[1]</sup> Homogeneous occupation of this orientation fiber also leads to a low anisotropy within the sheet plane. As the  $\gamma$ -fibre is mainly created during recrystallization after heavy cold rolling, this process is of high significance for applications of IF steel. Another important crystal orientation fiber is  $\langle 110 \rangle / \text{RD}$ . The latter is called  $\alpha$ -fibre and is formed typically when rolling bcc metals.

The problem with recrystallization of IF steels is related to the heterogeneity of the process. Figure 1 shows an example of a recrystallization process taken from a work by Raabe.<sup>[2]</sup> In this case, recrystallization evolved in a strongly heterogeneous way throughout the material. In the lower part of the picture, recrystallization has not taken place at all, whereas, in the upper part, two different recrystallization regimes are visible, showing different grain sizes. All three different kinds of microstructure, as expected, display different mechanical behaviors and lead to unwanted surface effects (such as orange peel structure) during deep-drawing operations. In order to understand and predict phenomena such as the one shown in Figure 1, it is necessary to improve our knowledge of the recrystallization process. The basic problem in this context is understanding which features of the microstructure enable nucleation for the recrystallization process.

It has been well established that the ability to form a nucleus is strongly dependent on the orientation of the material<sup>[3]</sup> and it is therefore important to study the local orientation distribution and microstructure with high spatial resolution. EBSD applied in a high-resolution scanning electron microscope (SEM) is the most appropriate tool for this task as it gives both high resolution and large observable areas. In this communication we describe a study of the recrystallization progress in IF steel. The deformed and several partially recrystallized states are characterized mainly by EBSD investigations. TEM is also used to study details of the deformed microstructure.

**Experimental:** The EBSD measurements were carried out with a field emission SEM (JEOL JSM 6500 F) equipped with a TSL EBSD system and a Digiview CCD camera. The SEM was operated at an accelerating voltage of 15 kV. Samples were prepared by grinding and polishing. The samples were etched for a few seconds, using a solution of 10:1  $\text{H}_2\text{O}_2$ :HF. The etching process was stopped by using pure  $\text{H}_2\text{O}_2$ . As the microstructure of deformed IF steel shows quite small structures, the EBSD measurements were performed with a step size of 0.1 or 0.15  $\mu\text{m}$ . In order to the use of wrongly indexed orientations, data points with a confidence index lower than

[\*] I. Thomas, Dr. S. Zaefferer, Prof. D. Raabe  
Max-Planck-Institut für Eisenforschung  
Max-Planck-Strasse 1, D-40237 Düsseldorf (Germany)  
E-mail: thomas@mpie.de  
I. Thomas, Dr. F. Friedel  
Thyssen Krupp Stahl  
D-47161 Duisburg (Germany)

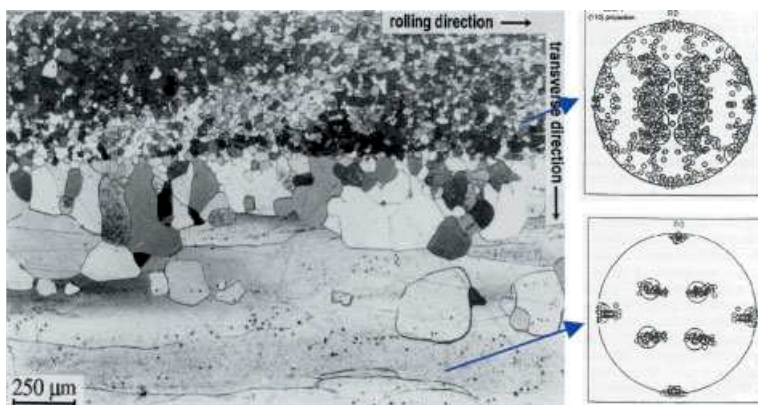


Fig. 1. Normal plane view of a low-carbon steel, 90% cold rolled and annealed for 120 s at 1000 K. The resulting microstructure is highly heterogeneous.

0.1 were removed from the EBSD data. These bad data points appear as black points in the EBSD maps.

The TEM investigations were carried out on a Phillips TEM CM20 operating at an accelerating voltage of 200 kV. Although rolled samples should generally be observed in transverse section with the TEM, normal sections were used for our investigation because of the very small thickness of the samples. The samples were thinned by electropolishing with a Struers Tenupol double jet at 60 V and 13° C. A solution of 95% CH<sub>3</sub>COOH and 5% HClO<sub>4</sub> was used as electrolyte. For the determination of crystal orientations with the TEM, Kikuchi diffraction has been used.

To investigate the partially recrystallized state, some of the cold rolled specimens were annealed in a muffle furnace. The samples were placed in the furnace in a protective atmosphere (95% N<sub>2</sub>; 5% H<sub>2</sub>) and were immediately quenched after reaching the desired temperature. The furnace temperature was set to 800° C during this procedure. In this way, a series of samples, ranging from cold rolled to fully recrystallized was produced.

*Characterization of the Deformed Microstructure:* The microstructure of the 75% cold rolled specimen, as revealed by EBSD measurements, is shown in Figure 2. Figure 2a shows an inverse pole figure map in which the detected orientations are color coded with reference to the normal direction of the sample. In Figure 2b, two different orientation classes ( $\alpha$ - and

$\gamma$ -fibre orientations) are highlighted in yellow and green respectively. As mentioned earlier, these two orientation fibers play an important role in recrystallization of IF steel as a texture dominated by  $\alpha$ -fibre develops during rolling and the fraction of  $\gamma$ -fibre orientations is increasing during recrystallization.<sup>[3]</sup> In the cold rolled material shown in Figure 2, 41% of the area observed consists of  $\alpha$ -fibre orientations, whereas 27% can be assigned to the  $\gamma$ -fibre. Finally, Figure 2c provides the image quality map of the area measured and, additionally, some classification of the observed grain boundaries. Grain boundaries separating grains with a misorientation of 2–5° are colored in blue, 5–15° in red, and greater than 15° in green.

Three different types of microstructure can be identified from the maps in Figure 2. The first type, colored in yellow in Figure 2b, consists of  $\alpha$ -fibre orientations. In these areas, no grain or subgrain boundaries are visible. In Figure 3, two misorientation profiles extracted from the data presented in Figure 2 are shown. Profile B points out the typical properties of  $\alpha$ -fibre orientations. The misorientation between neighboring points of the measurement (red line in Fig. 3) is always less than 2° in these areas, but the misorientations accumulate over longer distances (blue line in Fig. 2), up to 7° over a distance of 5  $\mu$ m.

The second type of microstructure is made up of  $\gamma$ -fibre orientations, which are green in Figure 2b. In these regions, low-angle grain boundaries separating subgrains with misorientations less than 15° are found. Concerning misorientation profile A in Figure 3, it can be seen that much higher misorientations between neighboring measurement points can be found here. The example shows values up to 10°. On the other hand, the misorientations do not seem to accumulate in  $\gamma$ -fibre orientations.

The third type of microstructure, visible as white areas in Figure 2b, contains many different orientations that cannot be assigned to  $\alpha$ - or  $\gamma$ -fibre orientations. For example, crystal orientations such as {120}<632>, {362}<311>, and {110}<221> are found here. In these areas, clear subgrain structures with a subgrain size of about 1  $\mu$ m can be observed. The boundary map (Fig. 2c) shows that these subgrains

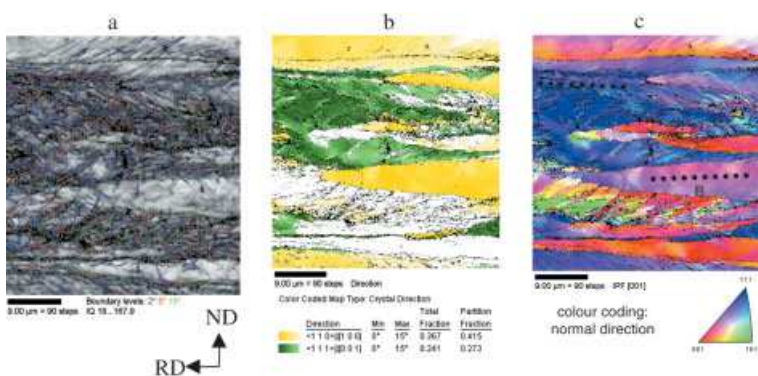


Fig. 2. EBSD measurements of a cold rolled sample: a) inverse pole figure map with reference to normal direction; b) coding of  $\alpha$ - and  $\gamma$ -fibre orientations in yellow and green respectively; c) image quality map with color-coded grain boundaries (blue = 2–5° misorientation, red = 5–15°, green = > 15°) [2].

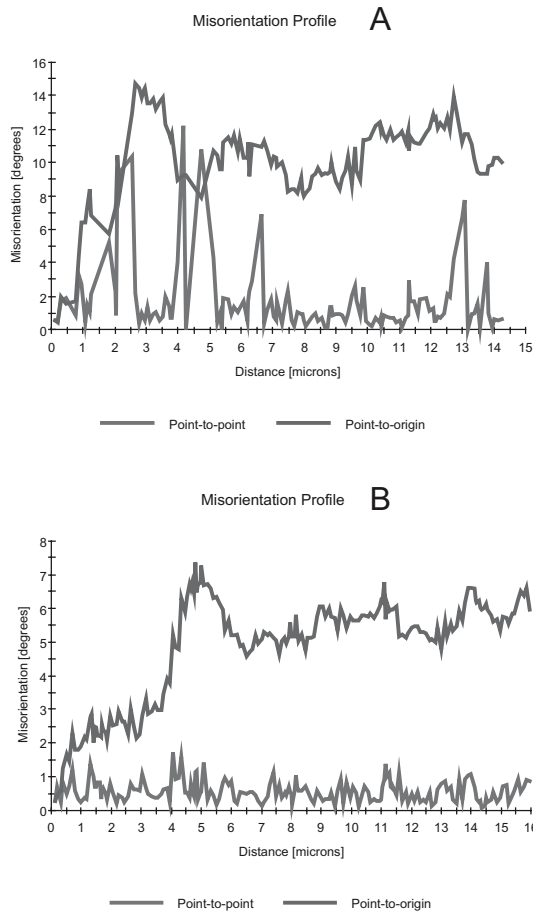
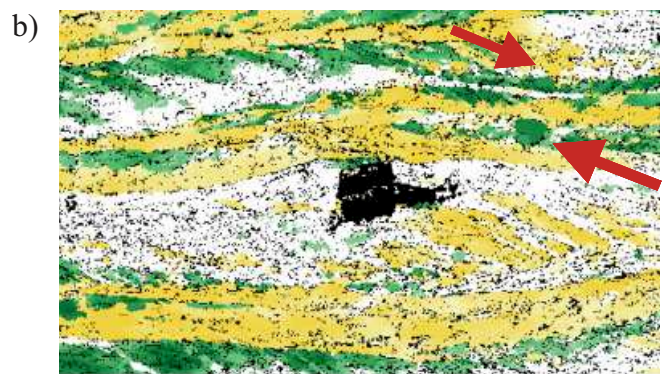
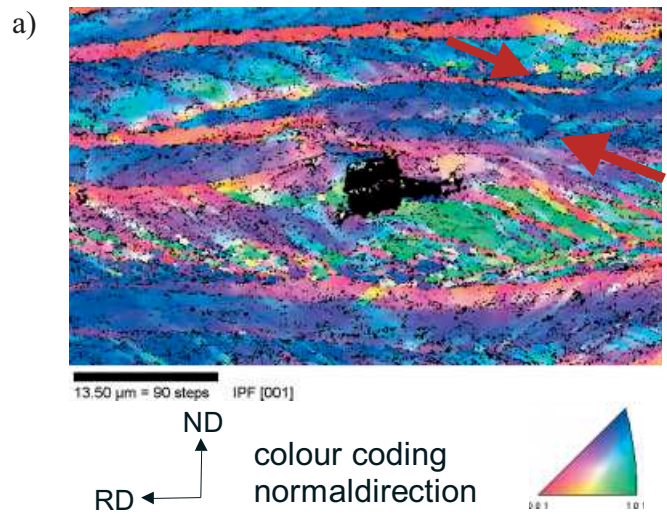


Fig. 3. Misorientation profiles taken from the positions marked in Figure 2a. Profile A shows the typical behavior found in  $\gamma$ -fibre, profile B in  $\alpha$ -fibre orientations.

are separated by some high-angle grain boundaries (misorientation  $> 15^\circ$ ).

*The Annealing Behaviour:* In this section, the results provided by two samples after annealing up to early states of recrystallization will be discussed.

The first sample was annealed for 2.5 min and quenched after a temperature of  $650^\circ\text{C}$  had been reached. Figure 4 shows results from an EBSD measurement carried out on a longitudinal section of this sample. The black area in the center of these maps indicates unreliable indexing results, which have been removed from the data. This wrong indexing was caused by a second-phase particle, which will be disregarded in this context. As this sample was annealed only for a short time, the characterization of the three different types of microstructure mentioned above is still valid in this case. At the positions marked by red arrows, however, three newly recrystallized grains are found. The image quality within these grains is much higher than for the matrix, indicating a lower dislocation density within the growing grains. The grains are surrounded by high-angle grain boundaries ( $> 15^\circ$ ). The lower arrow points out one larger recrystallized grain showing orientation  $\{111\}\langle 221 \rangle$ ; it can thus be assigned to a  $\gamma$ -fibre. This grain is positioned within an orientation gradient. According to older literature on recrystallization,<sup>[2]</sup> nuclei with



Color Coded Map Type: Crystal Direction

Direction	Min	Max	Total Fraction	Partition Fraction
$\langle 110 \rangle \parallel [100]$	$0^\circ$	$15^\circ$	0.406	0.478
$\langle 111 \rangle \parallel [001]$	$0^\circ$	$15^\circ$	0.176	0.207

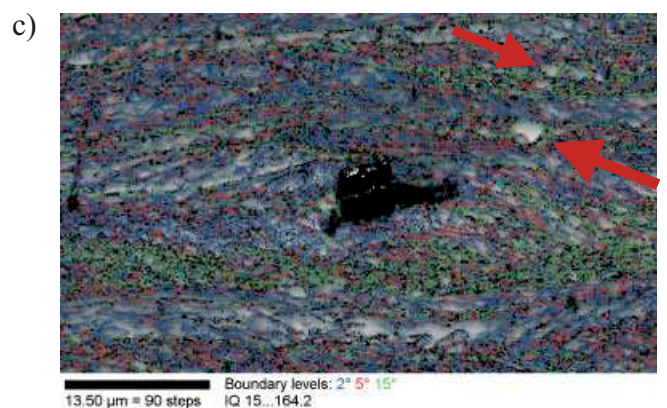


Fig. 4. EBSD results provided by a sample annealed for 2.5 min up to a temperature of  $650^\circ\text{C}$ . The red arrow marks the position of a nucleus growing from  $\gamma$ -fibre orientations. (For explanation of maps see Fig. 2).

$\gamma$ -fibre orientations should be expected. On the other hand, two other nuclei can also be found in this map and they are

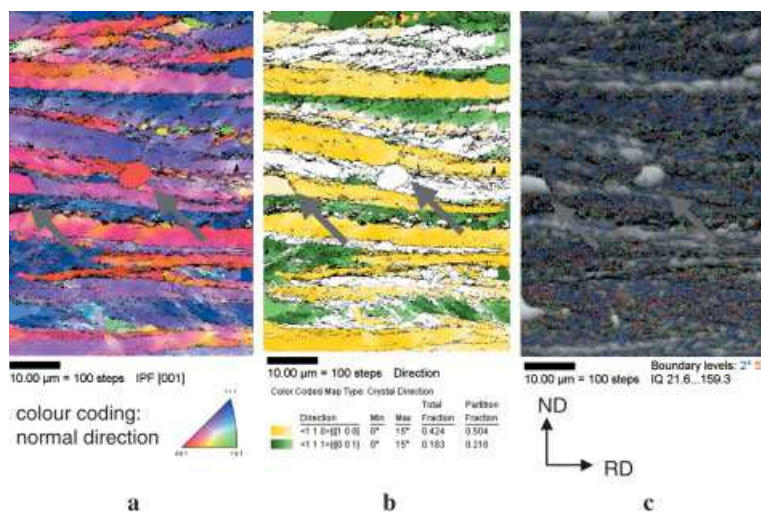


Fig. 5. EBSD results provided by a sample annealed for 3 min up to a temperature of 680 °C. The red arrows point out two nuclei that do not belong to  $\alpha$ - or  $\gamma$ -fibres. Additionally several nuclei with  $\gamma$ -fibre orientations can be seen in the upper part of the picture. (For explanation of maps see Fig. 2).

not  $\gamma$ -fibre oriented. The upper arrow marks two small grains with the orientations  $\{110\}\langle 110\rangle$  ( $\alpha$ -fibre oriented) and  $\{120\}\langle 210\rangle$  (neither  $\alpha$ - nor  $\gamma$ -fibre oriented). They are growing from a similarly oriented area of the deformed matrix.

The second sample was annealed for 3 min and quenched after it had reached a maximum temperature of 680 °C. Results obtained from this sample are shown in Figure 5. Several nucleation events have taken place in this sample that was annealed for a slightly longer time. The growing nuclei are easily identified by the higher image quality in their interior and by the surrounding high-angle grain boundaries.

In the upper part of the map five grains with  $\gamma$ -fibre orientations are found. Their orientations are  $\{111\}\langle 582\rangle$ ,  $\{111\}\langle 211\rangle$ ,  $\{111\}\langle 321\rangle$ , and  $\{111\}\langle 110\rangle$ . The last orientation is found twice and belongs to both  $\alpha$ - and  $\gamma$ -fibre.

Some recrystallized grains can also be found here that cannot be assigned to  $\alpha$ - or  $\gamma$ -fibre. They are identified by red arrows and their orientations are  $\{010\}\langle 100\rangle$  and  $\{010\}\langle 201\rangle$ .

**Summary of EBSD Results:** The deformed microstructure of cold rolled Ti-alloyed IF steel has been classified in three groups. The first consists of  $\alpha$ -fibre orientations ( $\langle 110\rangle//RD$ ). The EBSD maps show continuous orientation gradients in these areas and no grain boundaries with misorientations greater than 2° are detected. During annealing no significant changes in the microstructure of these areas are observed. The second kind is made up of  $\gamma$ -fibre orientations. At these locations, high values of point-to-point misorientation are determined by EBSD and clearly defined low-angle grain boundaries (< 15°) are detected. Nucleation from these areas is frequently observed during the annealing process. The third type of deformed microstructure consists of a lot of different orientations. Quite clear subgrain structures are observed at some locations. Some of these “subgrains” are separated by high-angle grain boundaries. This could be important because high-angle grain boundaries have higher

mobility and therefore enable recrystallization. During annealing, some nuclei originating from these areas have been found.

The first two types of microstructure ( $\alpha$ - and  $\gamma$ -fibre) are well known in literature<sup>[4]</sup> and their typical behavior has been confirmed by our measurements. In contrast, no literature on the third type of microstructure could be found. As there are high-angle grain boundaries observed in the deformed state, these locations could play a role in the recrystallization process.

**TEM Investigations:** The EBSD investigation of deformed  $\alpha$ -fibre orientations presented above shows continuous orientation gradients without any subgrains, whereas subgrains are found in  $\gamma$ -fibre orientations. In order to determine the cell morphology and the misorientations between the cells with higher accuracy and especially to take a closer look at the continuous orientation gradients found in the EBSD data, samples for TEM investigations

were prepared from the cold rolled material in normal section. In Figure 6, a TEM image of an area of  $\alpha$ -fibre orientations is shown. In contrast to the EBSD maps discussed above, a subgrain structure is visible. The subgrains have a size of about 1  $\mu$ m and are separated by diffuse boundaries consisting of wide dislocation walls, but can still be clearly identified. Neighboring subgrains show misorientations of 1–4.5°. These structures are obviously “smeared out” with our EBSD system due to limited spatial and angular resolution. When the incident electron beam hits the sample, the electrons are scattered within the material and the electrons used for EBSD are backscattered from a certain volume of the sample. If there is any grain boundary or dislocation wall inside this volume, the diffraction pattern detected originates from two different crystal orientations. Since these neighboring subgrains or cell structures usually show only little misorientations, the bands in the resulting diffraction pattern are broadened. This will lead the EBSD software to average between the two different crystal orientations and no clear grain boundary will appear in the related orientation mapping. The situation appears quite different in the TEM where the elec-

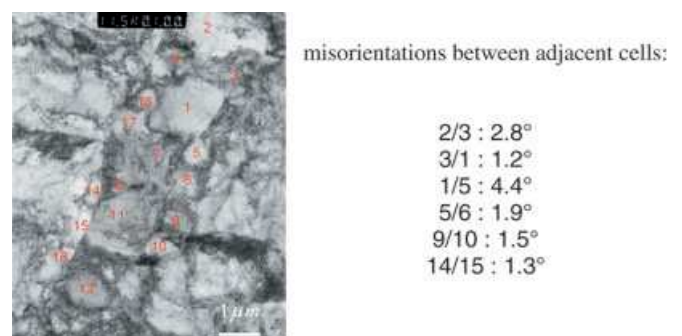
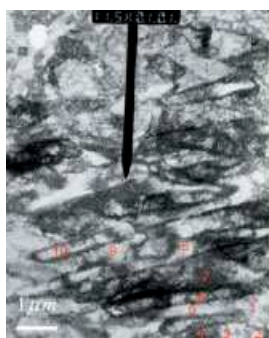


Fig. 6. TEM image of Ti-alloyed IF steel in normal section. The image was taken from an area with  $\alpha$ -fibre orientations. In contrast to EBSD-measurements, a very clear subgrain structure is visible.



Misorientations between adjacent cells:

1/2	: 1.7°
2/3	: 2.8°
3/4	: 5.3°
5/6	: 5.8°
6/7	: 5.8°
7/8	: 2.3°
9/10	: 4.5°

Fig. 7. TEM image of Ti-alloyed IF steel in the normal section. The image was taken from an area with  $\gamma$ -fibre orientations.

tron diffraction pattern stems from a significantly smaller volume than in the SEM. Additionally, dislocations are visible with the TEM and so localization of subgrains or cell structures is much easier.

A TEM image of  $\gamma$ -fibre orientations is shown in Figure 7. Subgrain structures are visible here too. However, in this case, the subgrains have a longitudinal shape and are separated by much sharper boundaries. The misorientations between neighboring subgrains are significantly higher as compared to the  $\alpha$ -fibre structures. Values of about 1.5–6° were found. Obviously these structures can be resolved by the EBSD system because they show sharper boundaries and higher misorientations than  $\alpha$ -fibre subgrains.

This comparison of EBSD results with TEM observations shows that not all subgrain structures are clearly resolved by the EBSD system. In this context, it is very useful to take additional information into account. For example, images provided by a backscatter detector often show cell structures at places where an orientation map only shows continuous orientation gradients. This indicates that using both methods (EBSD + SEM with strong orientation contrast) in combination can prevent misinterpretation of EBSD data.

Received: May 13, 2003

## Recrystallization and Texture in a Ferritic Stainless Steel: an EBSD Study\*\*

By Chad W. Sinclair,\* Florence Robaut, Laurent Maniguet, Jean-Denis Mithieux, Jean-Hubert Schmitt, and Yves Brechet

The recrystallization behavior of laboratory-processed AISI409 ferritic stainless steel sheet has been studied with a focus on texture inhomogeneity and “sluggish” recrystallization kinetics. This communication focuses primarily on observations made by electron backscatter diffraction (EBSD) in the scanning electron microscope (SEM). Pronounced texture gradients were observed in some grain orientations and correlated with the deformation-induced substructure. The strong pinning of some boundaries has been linked, not only to textural effects, but also to the precipitation of fine titanium carbonitrides.

Tailoring the physical and mechanical properties of steels through careful engineering of microstructure and texture has been responsible for many of the recent developments in light-weight, high-strength, and highly formable alloys. Demands for further improvements in material properties require ever more sophisticated descriptions of microstructure evolution under complex processing paths. Widespread availability of new techniques, such as EBSD, are now being used to provide a fully quantitative link between microstructure, texture, and mechanical properties. Of the many properties that must be controlled via processing, optimization of formability continues to be a priority for ferritic steel producers. Control of plastic anisotropy via the bulk texture of the final product is crucial in this regard and consequently has been heavily studied, particularly for carbon steels.<sup>[1]</sup> While

- [1] J. F. Held, *Mechanical Working and Steel Processing IV* (Ed.: D. A. Edgecombe), American Institute of Mining, Metallurgical and Petroleum Engineers, New York 1965.
- [2] D. Raabe, *Steel Res.* **1995**, 66, 222.
- [3] W. B. Hutchinson, *Acta Metall.* **1989**, 37, 1047.
- [4] H. Regle, in *Proc. First Joint Int. Conf. on Recrystallization and Grain Growth, Aachen, 2001*, (Eds: G. Gottstein, D. A. Molodow), Springer, Berlin 2001.

[\*] Dr. C. W. Sinclair  
Department of Metals and Materials Engineering  
University of British Columbia  
Vancouver BC V6T 1Z4 (Canada)

Dr. F. Robaut, Dr. L. Maniguet  
CMTC-INPG  
St. Martin d'Hères (France)

Dr. J.-D. Mithieux, Dr. J.-H. Schmitt  
CRI R&D Groupe Arcelor  
Isbergues (France)

Prof. Y. Brechet  
LTPCM-INPG  
St. Martin d'Hères (France)

[\*\*] One of the authors (CWS) would like to acknowledge fruitful discussions with D. Weygand and J. Lepinoux, and financial assistance from NSERC via a PDF scholarship.